



# Atomic Force Microscope with an Adjustable Probe Direction and Integrated Sensing and Actuation

Janik Schaude<sup>1</sup> · Tino Hausotte<sup>1</sup>

Received: 23 March 2022 / Revised: 10 May 2022 / Accepted: 11 May 2022 / Published online: 11 June 2022  
© The Author(s) 2022

## Abstract

This article presents the application and evaluation of a cantilever with integrated sensing and actuation as part of an atomic force microscope (AFM) with an adjustable probe direction, which is integrated into a nano measuring machine (NMM-1). The AFM, which is operated in closed-loop intermittent contact mode, is based on two rotational axes that enable the adjustment of the probe direction to cover a complete hemisphere. The axes greatly enlarge the metrology frame of the measuring system by materials with a comparatively high coefficient of thermal expansion, which ultimately limits the achievable measurement uncertainty of the measuring system. Thus, to reduce the thermal sensitivity of the system, the redesign of the rotational kinematics is mandatory. However, in this article, some preliminary investigations on the application of a self-sensing cantilever with an integrated micro heater for its stimulation will be presented. In previous investigations, a piezoelectric actuator has been applied to stimulate the cantilever. However, the removal of the piezoelectric actuator, which is enabled by the application of a cantilever with an integrated micro heater, promises an essential simplification of the sensor holder. Thus, in the future it might be possible to use materials with a low coefficient of thermal expansion, which are often difficult to machine and therefore only allow for rather simple geometries. Furthermore, because of the creepage of piezoelectric actuators, their removal from the metrology frame might lead to improved metrological characteristics. As will be shown, there are no significant differences between the two modes of actuation. Therefore, the redesigned rotational system will be based on the cantilever with integrated sensing and actuation.

**Keywords** Atomic force microscopy · Tilting AFM · Piezoresistive cantilever · Self-actuated cantilever · Nano measuring machine

## 1 Introduction

Nearly four decades ago, Norio Taniguchi forecasted the future development of machining accuracy by extrapolating historical data and predicted that by the turn of the millennium, ultraprecision machining could achieve an accuracy of 1 nanometer, or one-millionth of a millimeter [1]. Now, the future has become the past, and Taniguchi's forecasts have been proven to be correct [2–4]. In particular, the ultraprecise production of miniaturized, truly three-dimensional structures [5] or mesoscale components with microscale features [6] was made possible. These ultraprecise production

processes are applied in many different areas, such as optics to produce free-form surfaces [7, 8], power engineering to fabricate miniaturized turbine impellers [9], medicine to manufacture penetrating microelectrodes [10], and the consumer industry to achieve decorative effects [11].

For dimensional metrology, this still-ongoing trend of miniaturization was and still is a challenge because simple downscaling of established procedures is impossible due to scaling effects, i.e., effects negligible in the mesoscale become crucial in the microscale and nanoscale [12]. Upcoming, highly accurate positioning systems, like the Nano Measuring Machine NMM-1 [13] and shortly thereafter the Ultra Precision Coordinate Measuring Machine [14], which both fulfil the Abbe comparator principle [15] or rather the deduced Bryan principle [16] enabled positioning within a three-dimensional volume over several millimeters in each axis with an uncertainty of several nanometers. Nevertheless, because of the lack of suitable sensors, there

---

✉ Janik Schaude  
janik.schaude@fmt.fau.de

<sup>1</sup> Chair of Manufacturing Metrology, Friedrich-Alexander-Universität Erlangen-Nürnberg, Nögelsbachstr. 25, 91052 Erlangen, Germany

was, and partly still is, a metrological gap in performing nanometrological measurements on truly three-dimensional structures [17, 18].

The approaches used to fill the gap in three-dimensional nanometrology can be classified into two categories [19]: In a top-down approach, three-dimensional but not nanometrological sensor systems have been miniaturized and aligned to comply with the demands of nanometrology. A current review of such systems can be found in [20]. Conversely, in a bottom-up approach, highly accurate and nanometrological but, in principle, one-dimensional sensors mainly applied in surface metrology, such as the atomic force microscope (AFM) [21], have been tailored to be applicable for three-dimensional measurements.

The second approach can be further subdivided into approaches modifying the sensor and approaches modifying the positioning system. Moreover, as the semiconductor industry needs to determine critical dimensions, such as feature width, edge profile, or line edge roughness [22], several modified AFM cantilevers, e.g., with a boot-shaped tip [23], a further glued cantilever [24], a glued probing sphere [25], or particularly long cantilevers for the measurement of high aspect ratios [26, 27], have been developed. An alternative for the measurement of vertical or near-vertical surface features, or surfaces with a varying surface normal, is to apply a modified positioning system and introduce an inclination between the measuring object and the cantilever, which can be done by adjusting the sample [28–31] or tilting the cantilever [32–36] in one direction. A current review of the application of the AFM to measure critical dimensions can be found in [37].

More versatile, at the FAU Erlangen-Nürnberg [38] and, more recently, at the TU Ilmenau [39], a rotational kinematics has been integrated into a NMM-1 to adjust the probe direction of a sensor in two directions, thereby enabling the conduction of truly three-dimensional measurements with a one-dimensional sensor. Examples are the integration of a fixed scanning tunneling microscope [40], an oscillating tunneling microscope [41], a fiber-optic distance sensor [42] or an AFM [43]. With the AFM, some preliminary investigations on the achievable measurement precision have already been reported [44, 45]. The sensor system achieves a certain noise level and a short-term measurement precision in the low single-digit nanometer range. Furthermore, the standard deviation of the measured height of a calibration grating, both placed within and tilted to the horizontal plane with the probe direction adjusted accordingly, is in the double-digit picometer range, with a mean value that is consistent with the nominal step height. However, the empirically determined thermal sensitivity of the sensor system, which is mainly attributable to the rotational kinematics that greatly enlarges the metrology frame of the measuring system by materials with a comparatively high coefficient of thermal

expansion, is 1.3 nm/mK. Thus, the achievable long-term measurement precision, which is particularly crucial when conducting complex and time-consuming measurements, is limited.

To reduce the thermal sensitivity of the system, the redesign of the rotational kinematics is mandatory. However, for the moment, some preliminary investigations on the application of a commercially available, self-sensing cantilever with an integrated micro heater for its stimulation will be presented. In previous investigations, a piezoelectric actuator has been applied to stimulate the cantilever. However, the removal of the piezoelectric actuator, which is enabled by the application of a cantilever with an integrated micro heater, enables an essential simplification of the sensor holder. Thus, in the future it might be possible to use materials with a low coefficient of thermal expansion, which nevertheless are often difficult to machine and therefore allow for only rather simple geometries. Furthermore, because of the creepage of piezoelectric actuators [46], their removal from the metrology frame might lead to improved metrological characteristics.

A possible application of the redesigned sensor system is the highly accurate and nondestructive measurement of the crack length of a compact tension specimen according to the ASTM E 647-08 standard. Such specimens are applied in the experimental determination of the fracture mechanical parameters of clinchable metal sheets [47].

This paper is organized as follows: In Sect. 2, the measuring system is introduced. In Sect. 3, the metrological characteristics of the measuring system equipped with a cantilever with integrated sensing and actuation are investigated and compared with the previous system, including a piezoelectric actuator. In Sect. 4, a detailed analysis of the error sources contributing to the short-term precision is presented. Finally, in Sect. 5, the results are summarized and discussed, and an outlook is given.

## 2 Setup

The flexibility to adjust the probe direction of the AFM was achieved by utilizing the commercial SCL-Sensortech Piezo-Resistive Sensing & Active (PRSA) cantilever with a length of 110  $\mu\text{m}$ , a width of 48  $\mu\text{m}$ , and a silicon tip with a nominal radius of < 15 nm. Self-sensing methods, such as the piezoresistive deflection measurement [48], are compact but still provide a high signal-to-noise ratio similar to the commonly used optical beam deflection [49]. To reduce the contact forces and minimize the elastic or plastic deformations of the sample and tip, the cantilever was operated in intermittent-contact mode [50]. The micro heater applied to the cantilever stimulates it without the need for an external actuator [51]. As tip wear mainly occurs at the beginning of

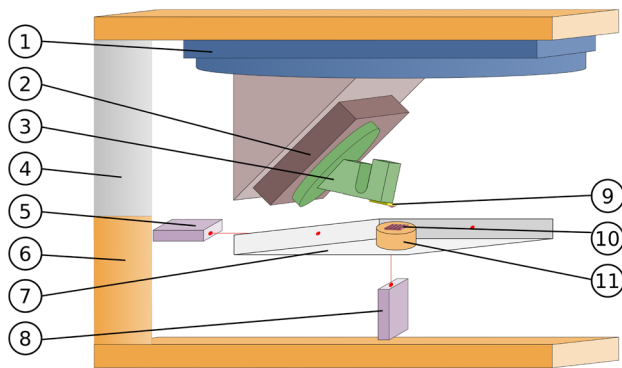


**Fig. 1** Simplified schematic of the setup: 1 first axis; 2 second axis; 3 sensor holder; 4 invar spacer; 5 y-interferometer; 6 Zerodur frame; 7 corner mirror; 8 z-interferometer; 9 piezoresistive cantilever; 10 measuring object; 11 spacer. Figure modified from [44]

the usage of a cantilever [52], several pre-scans have been conducted to ensure that the effect of tip wear is insignificant. All measurements have been conducted within a thermostating housing with a long-term temperature stability of 17 mK [53] and a set temperature of 20 °C.

## 2.1 Mechanical Design

The entire setup, shown schematically in Fig. 1, consisted of the first axis (1), i.e., the Aerotech ANT95R-180 with a positioning range of 180°, and the second axis (2), i.e., the SmarAct SR-2812 with a positioning range of 360° mounted under an angle of 45° to the first axis by an angle piece.

A sensor holder (3) connected the second axis to the socket of a piezoresistive cantilever (9) with integrated actuation. The entire setup was installed in the NMM-1 [54, 55] with a range of motion of 25 mm × 25 mm × 5 mm. The NMM-1 fulfills the Abbe comparator principle in all three coordinate axes by keeping the measuring system (i.e., three perpendicular homodyne Michelson interferometers fed by stabilized helium-neon lasers with a resolution of less than 0.1 nm each; two of them are shown, namely, 5 and 8) fixed and moving the measuring object (10). The measuring object was placed on a corner mirror (7), which defines the coordinate system of the NMM-1 and provides the three orthogonal measuring mirrors for the interferometers. The location of the tip of the cantilever at the intersection point of the three interferometers, the so-called Abbe point, would ensure the highest accuracy. Nevertheless, it limits the adjustment range of the probe direction to approximately half of a hemisphere, as the positioning range of the first axis is limited to approximately 90° to prevent collision with the corner mirror. To sustain the full positioning range, the sensor was located approximately 5 mm above the Abbe point. Therefore, a spacer (11) was used for the flat measuring object, and invar spacers (4) were used to enlarge the

Zerodur frame (6) of the NMM-1 to integrate the sensor system. However, the additional angle sensors and the angle control of the corner mirror around the *x*- and *y*-axes of the NMM-1 reduced the angular deviations during movement and thus any first-order deviations that arise because of the vertical distance to the Abbe point. A detailed explanation of the sensor holder is given in [45]. Figure 2 shows the sensor holder integrated into the NMM-1.

## 2.2 Signal Processing

During the experiments, probe sensor signal evaluation was conducted using the Zurich Instruments HF2LI lock-in amplifier. A sinus signal  $V_{\text{Ref}}$  was subjected to impedance conversion by the Analog Devices LT1206 current feedback amplifier and used to stimulate the micro heater on the cantilever with slightly less than half of the resonance frequency of the cantilever. The dissipated power can be calculated as follows:

$$P = \frac{V_{\text{Heater}}^2}{R}, \quad (1)$$

where  $V_{\text{Heater}}$  denotes the applied voltage and  $R$  denotes the ohmic resistance of the micro heater.  $P$  is proportional to the square of  $V_{\text{Heater}}$ . Therefore, the cantilever is stimulated near its resonance frequency [56]. The signal of the piezoresistive cantilever was amplified by the SCL-Sensortech commercial preamplifier. The amplified signal  $V_{\text{AFM}}$  was transduced to the lock-in amplifier, which calculated the phase-independent amplitude of the oscillation at the second harmonic of the driving signal,  $R_{\text{AFM}}$ .  $R_{\text{AFM}}$  is the measuring signal passed to the analog-to-digital converter (ADC) of the NMM-1 with a band limitation of 3 kHz to control the *x*-, *y*-, and *z*-axes according to the sensor orientation and current probing direction specified in the measuring command. Therefore, measurements were conducted in amplitude-controlled closed-loop intermittent-contact mode. The band limitation

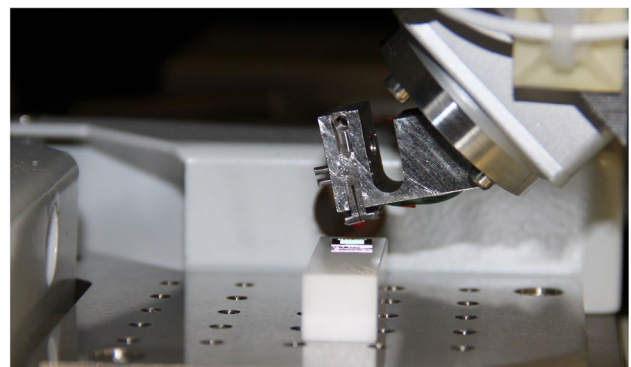


**Fig. 2** Setup integrated into the NMM-1



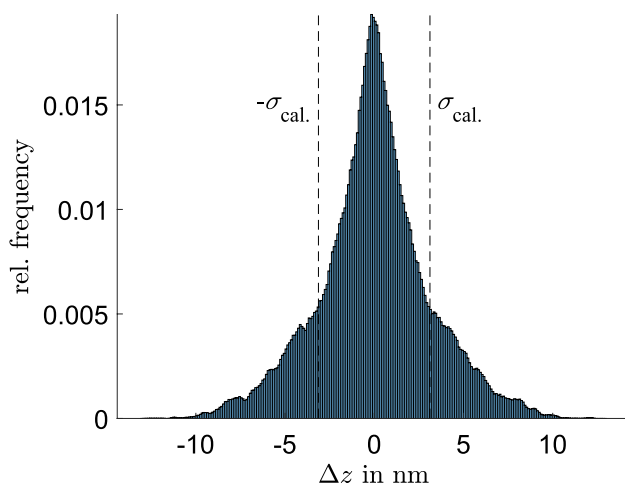


**Fig. 5**  $\Delta z$  as a histogram, with its standard deviation  $\sigma_{\text{calibration}}$ , which is 3.1 nm

The results are shown in Fig. 6. The three standard deviations of  $z_{\text{NMM}}$  are 2.4 nm (red), 2.5 nm (green), and 2.7 nm (blue). The combination of these values yields  $\sigma_{\text{standstill}}$ , which is 2.5 nm. This value is affected by thermal variations. Nevertheless, deducing the noise level as the standard deviation of  $d_{\text{AFM}}$  is possible as the controller compensates for the mainly temperature-induced low-frequency variations. The three standard deviations of  $d_{\text{AFM}}$  and thus  $\sigma_{\text{noise}}$  are 0.2 nm.

### 3.2 Long-Term Precision

Thus far, the investigations presented have been on a timescale of several minutes only. Nevertheless, complex measurements might last several hours. Thus, the precision of the sensor needs to be investigated on a longer timescale

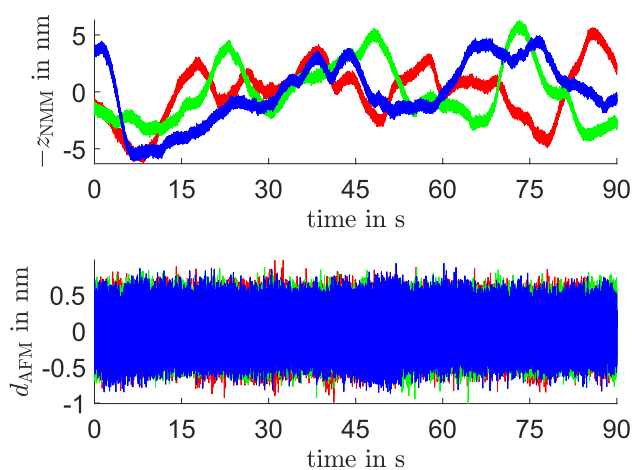


**Fig. 6** Three standstill measurements in closed-loop mode over 90 s. On the *upper panel*, an offset has been added to  $-z_{\text{NMM}}$  for illustrative purposes

as well. To determine the long-term (intermediate) measurement precision of the sensor, standstill measurements were conducted for 15 s every 10 min for several hours. The measured  $z$  value  $z_{\text{M}}$  was calculated using the following equation:

$$z_{\text{M}} = -z_{\text{NMM}} + d_{\text{AFM}} \quad (3)$$

For each 15 s-measurement, the offset was calculated as the mean of  $z_{\text{M}}$ . Between the measurements, the cantilever was withdrawn from the surface to prevent tip or sample damage. Figure 7 shows the mean of  $z_{\text{M}}$  over 18 h after stabilization. Within this period, the standard deviation of the offset,  $\sigma_{\text{long-term}}$ , is 6.6 nm.

### 3.3 Scans on a Calibration Grating

Closed-loop scans were conducted on a calibration grating (TGZ1 of NT-MDT), a type PPR material measure according to ISO 25178-70 [57] with a nominal step height of  $(21.4 \pm 1.5)$  nm. First, the measured values within the (negated) coordinate system of the NMM-1 were calculated according to Eq. (3). Afterward, the measured values were transformed into the workpiece coordinate system (WCS).

Because of the low-pass filtering associated with the calculation of  $d_{\text{AFM}}$ , as well as different ADCs used for the probe signal and interferometers of the NMM-1, latency between the signals of the interferometers and the probe signal is inevitable [43]. To avoid the effects caused by this latency, the scan velocity was set to only 5  $\mu\text{m/s}$ , and the point distance was set to 1 nm. The scan length was 90  $\mu\text{m}$ , and the step height was determined according to ISO 5436-1 [59]. The grating was placed within the  $xy$ -plane of the NMM-1. For the 30 scans on the same line at the measuring object, the mean of the determined step heights is 20.92 nm, which is consistent with the nominal value, and the associated standard deviation  $\sigma_{\text{step height}}$  is 59 pm. The high reproducibility of the scans is shown in Fig. 8, where 30 scans of the complete scan length (upper panel) and an irregularity on one step (lower panel) are depicted.

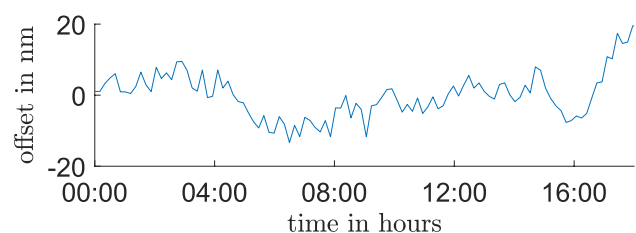


**Fig. 7** Long-term precision over 18 h

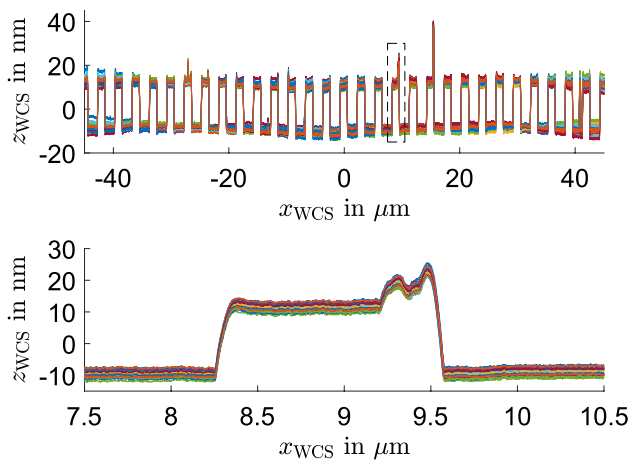


**Fig. 8** Thirty scans on the same line on the measuring object of the complete scan length (*upper panel*) and an irregularity on one step (*lower panel*) on the calibration grating

### 3.4 Comparison

Table 1 shows the results of the investigations on the metrological characteristics of the sensor system, both with actuation by a piezoelectric actuator and a cantilever with integrated micro heater. Apart from  $\sigma_{\text{standstill}}$ , the results are similar. However, thermal variations certainly influence all standard deviations, except for  $\sigma_{\text{noise}}$  and  $\sigma_{\text{step height}}$ . Because of the stochastic nature of thermal variations, ensuring that the results are equally influenced by these variations is impossible. To separate the effects of thermal variations from the determined short-term precision  $\sigma_{\text{calibration}}$ , the drift between the characteristic curves will be rectified in the subsequent section. However, for the sake of completeness, the obtained values for the offset-corrected  $\sigma_{\text{calibration}}$ ,  $\sigma_{\text{cal.,c}}$ , which is 0.4 nm for the cantilever with integrated micro heater and 0.5 nm for the actuation with a piezoelectric actuator, are also included in Table 1. Therefore, because the characteristics unaffected by thermal variations (i.e.,  $\sigma_{\text{cal.,c}}$ ,  $\sigma_{\text{noise}}$ , and  $\sigma_{\text{step height}}$ ) are nearly identical and the other characteristics are still similar, we can conclude that the metrological characteristics are not deteriorated by the

**Table 1** Comparison of both modes of actuation

Actuation	Integrated micro heater	Piezoelectric actuator [45]
$\sigma_{\text{calibration}}$	3.1 nm	3.5 nm
$\sigma_{\text{standstill}}$	2.5 nm	1.5 nm
$\sigma_{\text{noise}}$	0.2 nm	0.2 nm
$\sigma_{\text{step height}}$	59 pm	55 pm
$\sigma_{\text{long-term}}$	6.6 nm	6.5 nm
$\sigma_{\text{cal.,c}}$	0.4 nm	0.5 nm

application of a cantilever with integrated micro heater. Furthermore, as stated in the Introduction, the application of such a cantilever drastically simplifies the requirements for the sensor holder, thus enabling the application of materials with a low coefficient of thermal expansion, which are often difficult to machine.

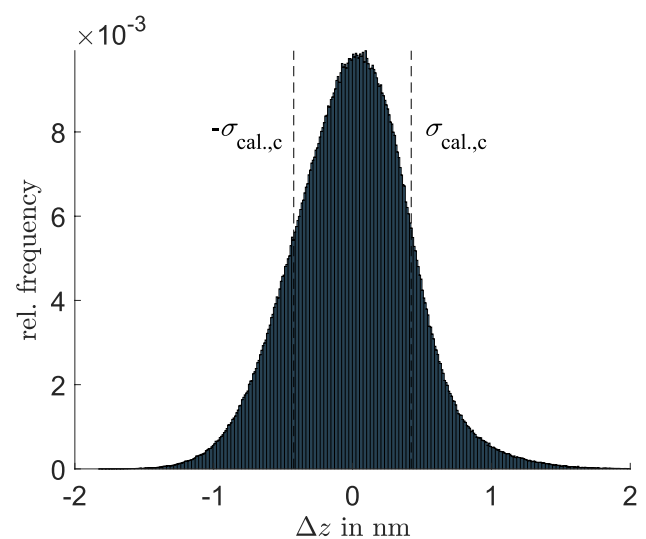
## 4 Error Sources

Figure 4 shows significant drifts between the calibrations and some systematic periodic deviations. As drifts between the calibrations are most likely attributable to low-frequency thermal variations, the effects of these drifts will be rectified in Sect. 4.1. The systematic periodic deviations may arise from nonlinearities of the interferometers of the NMM-1, which will be discussed in Sect. 4.2.

### 4.1 Drift

The offset of the characteristic curve  $d_{\text{AFM}}(R_{\text{AFM}})$  is equal to its polynomial coefficient of the order zero. By subtracting this offset from the values of  $z_{\text{NMM}}$  and recalculating the characteristic curve, we obtain the offset-corrected characteristic curve. After this correction, the offset-corrected  $\sigma_{\text{calibration}}$ ,  $\sigma_{\text{cal.,c}}$ , can be calculated, as discussed in the previous section. In Fig. 9,  $\Delta z$  of the offset-corrected calibrations is shown as a histogram, with its standard deviation  $\sigma_{\text{cal.,c}}$ , which is 0.4 nm.

Figure 10 shows  $\Delta z$  of the offset-corrected calibrations, where  $d_{\text{AFM}}(R_{\text{AFM}})$  is calculated using the first characteristic curve, and the residues of this characteristic curve are depicted in red. The subsequent section discusses how far



**Fig. 9**  $\Delta z$  of the offset-corrected calibrations as a histogram, with the standard deviation  $\sigma_{\text{cal.,c}}$ , which is 0.4 nm

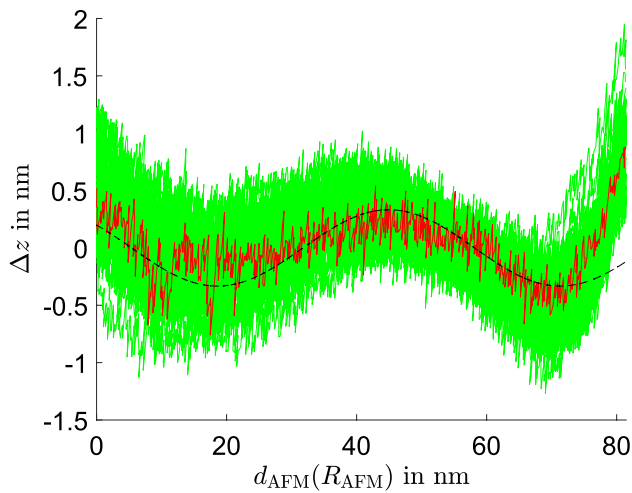


**Fig. 10** Deviations of the deflection of the cantilever to the offset-corrected  $z$  values of the NMM-1 for 50 calibrations. The residues of the first curve are shown in red. The dashed line denotes a sine curve with a periodicity of  $\lambda/12$

the remaining systematic deviations might arise from periodic nonlinearities of the  $z$ -interferometer of the NMM-1.

### 4.2 Periodic Nonlinearities of the $z$ -interferometer

To achieve directional sensitivity, as well as a resolution far below the laser’s wavelength  $\lambda$  with a homodyne interferometer, two signals with a phase shift of  $90^\circ$  are evaluated, which is also known as phase quadrature measurement [60]. However, because of the mismatched amplitude or offset of the signals, as well as a phase shift different from  $90^\circ$ , significant nonlinearities of the evaluated length values may occur, mainly with a periodicity of  $\lambda/2$  (in the case of a  $\lambda/2$ -interferometer) [61, p. 67 et seq.]. Peter Heydemann proposed the correction of these nonlinearities by fitting an ellipse to the quadrature signals and rectifying them onto a circle [62]. This procedure, known as the Heydemann correction, will be applied to the repeated, offset-corrected calibrations (cf. Fig. 10).

To determine the parameters of the ellipse of the  $z$ -interferometer, the stage of the NMM-1 has been moved 30 times for  $2\ \mu\text{m}$  in the  $z$ -direction with the cantilever being in free air just before the sample.  $z_{\text{NMM}}$  and the unprocessed quadrature signals  $Q_A$  and  $Q_B$  were recorded with a point distance of 1 nm. The equation of the ellipse is given by

$$A Q_A^2 + B Q_B^2 + C Q_A Q_B + D Q_A + E Q_B = 1, \tag{4}$$

where  $A, B, C, D,$  and  $E$  denote the coefficients of the equation of the ellipse. These coefficients are determined by fitting Eq. (4) to the measured data. With these coefficients, the relevant parameters of the ellipse, which are the phase

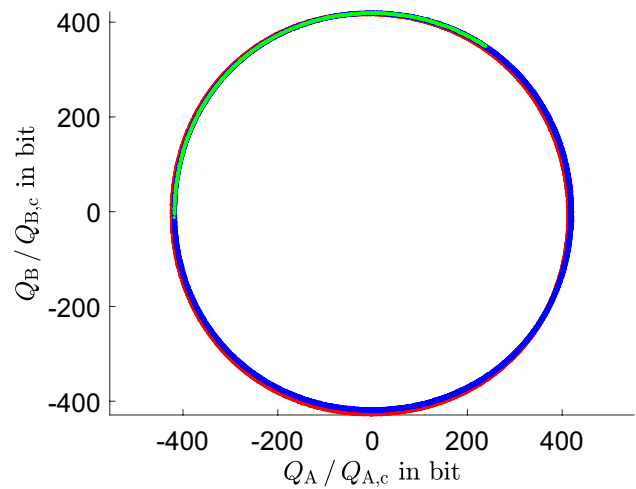


**Fig. 11** Uncorrected (red) and corrected (blue) quadrature signals of the  $z$ -interferometer of the NMM-1. Shown in green are the corrected quadrature signals of the calibrations

deviation  $\alpha$ , radius ratio  $r$ , offset of  $Q_A, O_A$ , and offset of  $Q_B, O_B$ , can be calculated using Eqs. (5)–(8).

$$\alpha = \arcsin\left(\frac{C}{\sqrt{4AB}}\right) \tag{5}$$

$$r = \sqrt{\frac{B}{A}} \tag{6}$$

$$O_A = \frac{2BD - CE}{C^2 - 4AB} \tag{7}$$

$$O_B = \frac{2AE - CD}{C^2 - 4AB} \tag{8}$$

In a final step, the corrected signals are obtained as follows [61, p. 69]:

$$Q_{A,c} = Q_A - O_A \tag{9}$$

$$Q_{B,c} = \frac{Q_{A,c} \cdot \sin(\alpha) + r(Q_B - O_B)}{\cos(\alpha)} \tag{10}$$

In Fig. 11, the uncorrected and corrected quadrature signals are shown in red and blue, respectively, and the corrected quadrature signals of the calibrations are shown in green. Notably, only approximately a quarter of the complete quadrature is covered when conducting the calibrations. From the quadrature signals, the length value is obtained by demodulation. The demodulated  $z$  value of the NMM-1 for the uncorrected quadrature signals is  $z_{\text{NMM}}$ , and the demodulated value for the corrected signal is  $z_{\text{NMM},c}$ . In Fig. 12, the

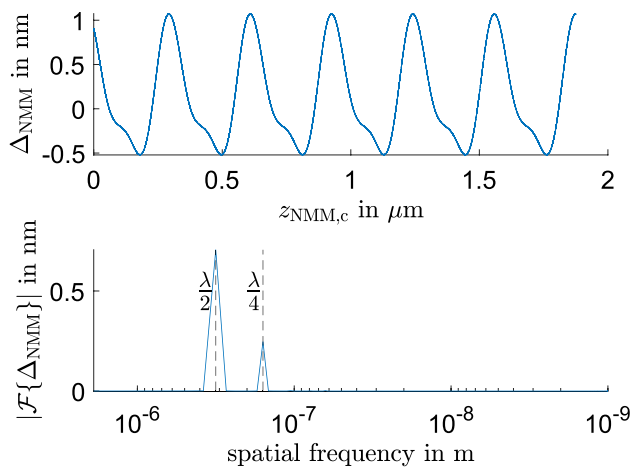


**Fig. 12** Error between the uncorrected and corrected length values of the  $z$ -interferometer of the NMM-1 (*upper panel*) and the Fourier spectrum of this error (*lower panel*)

error between both values, i.e.,  $\Delta_{\text{NMM}} = z_{\text{NMM}} - z_{\text{NMM,c}}$ , is shown. The amplitude of this error is approximately 1.5 nm. The spatial Fourier analysis revealed the main error components of  $\lambda/2$  and  $\lambda/4$ .

Nevertheless, as depicted in Fig. 10, the error on the characteristic curves has a wavelength of approximately  $\lambda/12$ , which is probably caused by reflections on the surface of the beam splitter cube in the measuring arm that leads to multibeam interference. Thus, it cannot be corrected by the Heydemann correction.

As the range of the characteristic curves is only approximately 80 nm, only approximately a quarter of the complete quadrature is covered when conducting the calibrations (cf. Fig. 11); thus, the error components of  $\lambda/2$  and  $\lambda/4$  might lead to systematic errors on the obtained characteristic curves, e.g., a mismatched inclination of the characteristic curve, but will not lead to errors between repeated calibrations conducted approximately at the same location of the quadrature. As a consequence, the Heydemann correction does not reduce  $\sigma_{\text{cal,c}}$  (which is still 0.4 nm), although it is in large part caused by the  $z$ -interferometer of the NMM-1.

## 5 Summary, Conclusion, and Outlook

In this article, the application of a cantilever with integrated sensing and actuation as part of an AFM with an adjustable probe direction has been shown and evaluated. Although the thermal sensitivity of the rotational axes limits the achievable long-term measurement precision to approximately 7 nm, when correcting these mainly thermally induced low-frequency errors, standard deviations in the picometer range are obtained. Systematic periodic errors are detected on the characteristic curve, with a standard deviation of

approximately 0.4 nm. As these errors occur in large part with a spatial frequency of  $\lambda/12$ , they are most likely caused by the interferometer. The comparison of the metrological characteristics of the sensor system equipped with the cantilever with an integrated micro heater for its stimulation and the sensor system equipped with a piezoelectric drive for its stimulation shows no significant differences between the two modes of actuation.

This study intended to verify the applicability of a cantilever with integrated sensing and actuation. This verification was successful; therefore, the redesign of the rotational kinematics will be based on the cantilever with integrated sensing and actuation. The removal of the piezoelectric actuator enables the simplification of the sensor holder and the application of materials with a low coefficient of thermal expansion. Furthermore, the effects of the creepage of piezoelectric actuators might have been erroneously attributed to thermal variations, so far. Thus, the removal of the piezoelectric actuator from the metrology frame might result in improved metrological characteristics, as well. Possible means to reduce the thermal sensitivity of the rotational kinematics are the application of smaller rotational axes or a different arrangement of the rotational axes. Placing the first axis above the Zerodur frame (cf. Fig. 1), reducing the length of the invar spacers, and connecting the first axis with the angle piece by materials with a low or even negative expansion coefficient, might result in compensating thermal expansions of the first axis and the remaining part of the sensor system.

**Acknowledgements** This project was funded by the Deutsche Forschungsgemeinschaft (DFG, German Research Foundation) -TRR 285 -Project-ID 418701707, subproject C05.

**Author Contributions** Conceptualization, JS and TH; methodology, JS and TH; software, JS and TH; validation, JS; formal analysis, JS; investigation, JS; resources, TH; data curation, JS; writing-original draft preparation, JS; writing-review and editing, TH; visualization, JS; supervision, TH; project administration, TH; funding acquisition, TH. All authors have read and agreed to the published version of the manuscript.

**Funding** Open Access funding enabled and organized by Projekt DEAL.

## Declarations

**Conflict of interest** The authors declare that they have no conflicts of interest.

**Open Access** This article is licensed under a Creative Commons Attribution 4.0 International License, which permits use, sharing, adaptation, distribution and reproduction in any medium or format, as long as you give appropriate credit to the original author(s) and the source, provide a link to the Creative Commons licence, and indicate if changes were made. The images or other third party material in this article are included in the article's Creative Commons licence, unless indicated



otherwise in a credit line to the material. If material is not included in the article's Creative Commons licence and your intended use is not permitted by statutory regulation or exceeds the permitted use, you will need to obtain permission directly from the copyright holder. To view a copy of this licence, visit <http://creativecommons.org/licenses/by/4.0/>.

## References

1. Taniguchi N (1983) Current status in, and future trends of, ultra-precision machining and ultrafine materials processing. *CIRP Ann* 32(2):573–582
2. Masuzawa T (2000) State of the art of micromachining. *CIRP Ann* 49(2):473–488
3. Geiger M, Kleiner M, Eckstein R, Tiesler N, Engel U (2001) Microforming. *CIRP Ann* 50(2):445–462
4. Byrne G, Dornfeld D, Denkena B (2003) Advancing cutting technology. *CIRP Ann* 52(2):483–507
5. Masuzawa T, Tönshoff HK (1997) Three-dimensional micromachining by machine tools. *CIRP Ann* 46(2):621–628
6. Uhlmann E, Mullany B, Biermann D, Rajurkar KP, Hausotte T, Brinksmeier E (2016) Process chains for high-precision components with micro-scale features. *CIRP Ann* 65(2):549–572
7. Gebhardt A, Steinkopf R, Scheiding S, Risse S, Damm C, Zeh T, Kaiser S (2010) MERTIS—optics manufacturing and verification. In: *Proceedings of SPIE*, vol 7808
8. Fang FZ, Zhang XD, Weckenmann A, Zhang GX, Evans C (2013) Manufacturing and measurement of freeform optics. *CIRP Ann* 62(2):823–846
9. Liu K, Peirs J, Ferraris E, Lauwers B, Reynaerts D (2008) Micro electrical discharge machining of Si<sub>3</sub>N<sub>4</sub>-based ceramic composites. In: *Proceedings of the 4th international conference on multi-material micro manufacture*, pp 161–166
10. Kamaraj AB, Sundaram MM, Mathew R (2013) Ultra high aspect ratio penetrating metal microelectrodes for biomedical applications. *Microsyst Technol* 19(2):179–186
11. Blondiaux N, Diserens M, Chauvy PF, Oudot B, Pugin R (2021) Manufacturing of hierarchically structured surfaces for decorative applications. In: *Proceedings of 21st EUSPEN international conference*, pp 119–120
12. Alting L, Kimura F, Hansen HN, Bissacco G (2003) Micro engineering. *CIRP Ann* 52(2):635–657
13. Jäger G, Manske E, Hausotte T, Büchner HJ (2000) Nanomessmaschine zur abbefehlerfreien Koordinatenmessung. *TM Tech Mess* 67(7–8):319–323
14. Ruijl T (2001) Ultra precision coordinate measuring machine—design, calibration and error compensation. Ph.D. thesis, Technische Universiteit Eindhoven
15. Abbe E (1890) Meßapparate für Physiker. *Zeitschrift für Instrumentenkunde* 10:446–448
16. Bryan JB (1979) The Abbé principle revisited: an updated interpretation. *Precis Eng* 1(3):129–132
17. Hansen HN, Carneiro K, Haitjema H, De Chiffre L (2006) Dimensional micro and nano metrology. *CIRP Ann* 55(2):721–743
18. Leach RK, Boyd R, Burke T, Danzebrink HU, Dirscherl K, Dziomba T, Gee M, Koenders L, Morazzani V, Pidduck A, Roy D, Unger WES, Yacoot A (2011) The European nanometrology landscape. *Nanotechnology* 22(6):062001
19. Weckenmann A, Peggs G, Hoffmann J (2006) Probing systems for dimensional micro- and nano-metrology. *Meas Sci Technol* 17(3):504–509
20. Michihata M (2022) Surface-sensing principle of microprobe system for micro-scale coordinate metrology: a review. *Metrology* 2(1):46–72
21. Binnig G, Quate CF, Gerber C (1986) Atomic force microscope. *Phys Rev Lett* 56(9):930–933
22. Yacoot A, Koenders L (2011) Recent developments in dimensional nanometrology using AFMs. *Meas Sci Technol* 22(12):122001
23. Martin Y, Wickramasinghe HK (1994) Method for imaging sidewalls by atomic force microscopy. *Appl Phys* 64(19):2498–2500
24. Dai G, Wolff H, Weimann T, Xu M, Pohlenz F, Danzebrink HU (2007) Nanoscale surface measurements at sidewalls of nano- and micro-structures. *Meas Sci Technol* 18(2):334–341
25. Dai G, Wolff H, Danzebrink HU (2007) Atomic force microscope cantilever based microcoordinate measuring probe for true three-dimensional measurements of microstructures. *Appl Phys Lett* 91(12):121912
26. Lebrasseur E, Pourciel JB, Bourouina T, Masuzawa T, Fujita H (2002) A new characterization tool for vertical profile measurement of high-aspect-ratio microstructures. *J Micromech Microeng* 12(3):280–285
27. Peiner E, Doering L (2010) MEMS cantilever sensor for non-destructive metrology within high-aspect-ratio micro holes. *Microsyst Technol* 16(7):1259–1268
28. Garnæs J, Hansen P.E, Agersnap N, Davi I, Petersen J.C, Kühle A, Holm J, Christensen LH (2005) Determination of sub-micrometer high aspect ratio grating profiles. In: *Proceedings of SPIE*, vol 5878
29. Zhao XS, Sun T, Yan YD, Li ZQ, Dong S (2006) Measurement of roundness and sphericity of the micro sphere based on atomic force microscope. *Key Eng Mater* 315–316:796–799
30. Fouchier M, Pargon E, Bardet B (2013) An atomic force microscopy-based method for line edge roughness measurement. *Appl Phys* 113(10):104903
31. Oertel E, Manske E (2021) Radius and roundness measurement of micro spheres based on a set of AFM surface scans. *Meas Sci Technol* 32(4):044005
32. Dal Savio C, Dejima S, Danzebrink HU, Gotszalk T (2007) 3D metrology with a compact scanning probe microscope based on self-sensing cantilever probes. *Meas Sci Technol* 18(2):328–333
33. Jayanth GR, Jhiang SM, Menq CH (2008) Two-axis probing system for atomic force microscopy. *Rev Sci Instrum* 79(2):023705
34. Hua Y, Coggins C, Park S (2010) Advanced 3D metrology atomic force microscope. In: *IEEE/SEMI ASMC*, pp 7–10
35. Cho SJ, Ahn BW, Kim J, Lee JM, Hua Y, Yoo YK, Park S (2011) Three-dimensional imaging of undercut and sidewall structures by atomic force microscopy. *Rev Sci Instrum* 82(2):023707
36. Kizu R, Misumi I, Hirai A, Kinoshita K, Gonda S (2018) Development of a metrological atomic force microscope with a tip-tilting mechanism for 3D nanometrology. *Meas Sci Technol* 29(7):075005
37. Hussain D, Ahmad K, Song J, Xie H (2017) Advances in the atomic force microscopy for critical dimension metrology. *Meas Sci Technol* 28(1):012001
38. Schuler CA (2012) Erweiterung der Einsatzgrenzen von Sensoren für die Mikro- und Nanomesstechnik durch dynamische Sensornachführung unter Anwendung nanometeraufgelöster elektrischer Nahfeldwechselwirkung. Ph.D. thesis, Universität Erlangen-Nürnberg
39. Fern F (2020) Metrologie in fünfschigen Nanomess- und Nanopositioniermaschinen. Ph.D. thesis, Technische Universität Ilmenau
40. Schuler A, Weckenmann A, Hausotte T (2014) Setup and evaluation of a sensor tilting system for dimensional micro- and nanometrology. *Meas Sci Technol* 25(6):064010

41. Schuler A, Hausotte T, Sun Z (2015) Micro- and nanocoordinate measurements of micro-parts with 3-D tunnelling current probing. *J Sens Sens Syst* 4(1):199–208
42. Timmermann M, Weinert B, Schuler A, Loderer A, Hausotte T (2015) Fiber-optical 3-D measurement of highly curved free-form surfaces. In: 15th Int. Conf. on Met. & Props. of Eng. Surf
43. Schaude J, Albrecht J, Klöpzig U, Gröschl AC, Hausotte T (2019) Atomic force microscope with an adjustable probe direction and piezoresistive cantilevers operated in tapping-mode. *TM Tech Mess* 86(S1):12–16
44. Schaude J, Hausotte T (2021) Investigations on the measurement precision of an atomic force microscope with an adjustable probe direction. In: Proceedings of 21st EUSPEN international conference
45. Schaude J, Fimushkin M, Hausotte T (2021) Redesigned sensor holder for an atomic force microscope with an adjustable probe direction. *Int J Precis Eng Manuf* 22(9):1563–1571
46. Hegewald T (2007) Modellierung des nichtlinearen Verhaltens piezokeramischer Aktoren. Ph.D. thesis, Universität Erlangen-Nürnberg
47. Weiß D, Schramm B, Kullmer G (2020) Development of a special specimen geometry for the experimental determination of fracture mechanical parameters of clinchable metal sheets. *Procedia Struct Integr* 28:2335–2341
48. Tortonese M, Yamada H, Barrett R.C, Quate C.F (1991) Atomic force microscopy using a piezoresistive cantilever. In: TRANSDUCERS '91: international conference on solid-state sensors and actuators. Digest of Technical Papers, pp 448–451
49. Dukic M, Adams JD, Fantner GE (2015) Piezoresistive AFM cantilevers surpassing standard optical beam deflection in low noise topography imaging. *Sci Rep* 5:16393
50. Zhong Q, Inniss D, Kjoller K, Elings VB (1993) Fractured polymer/silica fiber surface studied by tapping mode atomic force microscopy. *Surf Sci* 290(1–2):L688–L692
51. Ivanov T, Gotszalk T, Grabiec P, Tomerov E, Rangelow IW (2003) Thermally driven micromechanical beam with piezoresistive deflection readout. *Microelectron Eng* 67–68:550–556
52. Czerkas S, Dziomba T, Bosse H (2005) Comparison of different methods of SFM tip shape determination for various characterisation structures and types of tip. In: Wilkening G, Koenders L (eds) *Nanoscale calibration standards and methods: dimensional and related measurements in the micro- and nanometer range*, vol 23, 1st edn. WILEY-VCH, Weinheim, pp 311–320
53. Gröschl AC, Schaude J, Hausotte T (2019) Evaluation und Korrektur thermischer Driften eines hochfrequent fokusbandsmodulierten, fasergekoppelten konfokalen Punktsensors. *TM Tech Mess* 86(S1):117–121
54. Hausotte T, Percle B, Jäger G (2009) Advanced three-dimensional scan methods in the nanopositioning and nanomeasuring machine. *Meas Sci Technol* 20(8):084004
55. Hausotte T (2018) Interferometric measuring systems of nanopositioning and nanomeasuring machines. In: Proceedings of SPIE, vol 10678
56. Fantner GE, Burns DJ, Belcher AM, Rangelow IW, Youcef-Toumi K (2009) DMCMN: in depth characterization and control of AFM cantilevers with integrated sensing and actuation. *J Dyn Syst Meas Control* 131(6):061104
57. DIN EN ISO 25178-70:2014. Geometrical product specification (GPS)—surface texture: areal—part 70: material measures (ISO 25178-70:2014)
58. VDI/VDE 2656-1 (2019) Determination of geometrical quantities by using of scanning probe microscopes; Calibration of measurement systems. Beuth Verlag, Berlin
59. DIN EN ISO 5436-1:2000. Geometrical product specification (GPS)—surface texture: profile method; measurement standards—part 1: material measures (ISO 5436-1:2000)
60. Ellis JD (2014) Field guide to displacement measuring interferometry, 1st edn. SPIE Press, Washington
61. Hausotte T (2011) Nanopositionier- und Nanomessmaschinen - Geräte für hochpräzise makro- bis nanoskalige Oberflächen- und Koordinatenmessungen, 1st edn. Pro Business, Berlin
62. Heydemann PLM (1981) Determination and correction of quadrature fringe measurement errors in interferometers. *Appl Opt* 20(19):3382–3384



**Janik Schaude** has been a research associate at the Chair of Manufacturing Metrology since 2017. Since 2020, he is head of the chair's calibration laboratory. His main fields of studies are nanometrology, atomic force microscopy and optical metrology.



**Prof. Tino Hausotte** is head of the Chair of Manufacturing Metrology. His main fields of studies are the X-ray computed tomography in dimensional metrology, surface and coordinate metrology, micro- and nanometrology, photogrammetry and measurement uncertainty evaluation.